A Highly Photostable Hyperbranched Polyglycerol-Based NIR Fluorescence Nanoplatform for Mitochondria-Specific Cell Imaging

Chunhong Dong, Zhongyun Liu, Junqing Liu, Changzhu Wu, Falko Neumann, Hanjie Wang, Monika Schäfer-Korting, Burkhard Kleuser, Jin Chang, Wenzhong Li, Nan Ma,* and Rainer Haag**

Considering the critical role of mitochondria in the life and death of cells, non-invasive long-term tracking of mitochondria has attracted considerable interest. However, a high-performance mitochondria-specific labeling probe with high photostability is still lacking. Herein a highly photostable hyperbranched polyglycerol (hPG)-based near-infrared (NIR) quantum dots (QDs) nanoplatform is reported for mitochondria-specific cell imaging. Comprising NIR Zn-Cu-In-S/ZnS QDs as extremely photostable fluorescent labels and alkyl chain (C_{12})/triphenylphosphonium (TPP)-functionalized hPG derivatives as protective shell, the tailored QDs@hPG-C_{12}/TPP nanoprobe with a hydrodynamic diameter of about 65 nm exhibits NIR fluorescence, excellent biocompatibility, good stability, and mitochondria-targeted ability. Cell uptake experiments demonstrate that QDs@hPG-C_{12}/TPP displays a significantly enhanced uptake in HeLa cells compared to nontargeted QDs@hPG-C_{12}. Further co-localization study indicates that the probe selectively targets mitochondria. Importantly, compared with commercial deep-red mitochondria dyes, QDs@hPG-C_{12}/TPP possesses superior photostability under continuous laser irradiation, indicating great potential for long-term mitochondria labeling and tracking. Moreover, drug-loaded QDs@hPG-C_{12}/TPP display an enhanced tumor cell killing efficacy compared to nontargeted drugs. This work could open the door to the construction of organelle-targeted multifunctional nanoplatforms for precise diagnosis and high-efficient tumor therapy.

1. Introduction

Mitochondria, the powerhouse and suicidal weapon store inside most eukaryotic cells, exert both vital and lethal functions in physiological and pathological scenarios.[1] Mitochondria dysfunctions led to many human diseases.[2] Numerous mutations of mitochondrial DNA contribute to an increased risk of developing some malignancies.[3] Mitochondria in tumor cells are structurally and functionally different from the normal counterparts.[4] Compared with nonimmortalized normal cells, tumor cells are more susceptible to mitochondrial perturbations, which make mitochondria become attractive alternative targets for cancer therapeutics.[5] Mitochondrial-targeted treatment could achieve better anticancer effect and help to overcome multidrug resistance in tumor chemotherapy, representing a promising approach to eradicate chemotherapy-refractory cancer cells.[6] Despite great efforts have been

C. Dong, Dr. J. Liu, Dr. H. Wang, Prof. J. Chang
School of Life Sciences
School of Materials Science and Engineering
Tianjin Engineering Center of Micro-Nano Biomaterials and Detection-Treatment Technology
Collaborative Innovation Center of Chemical Science and Engineering
Tianjin University
Tianjin 300072, P. R. China
E-mail: jinchang@tju.edu.cn

Dr. Z. Liu
Key Laboratory of Coastal Environmental Processes and Ecological Remediation
Research Center for Coastal Environmental Engineering and Technology of Shandong Province
Yantai Institute of Coastal Zone Research
Chinese Academy of Sciences
Yantai, Shandong 264003, P. R. China

Dr. C. Wu, F. Neumann, Prof. N. Ma, Prof. R. Haag
Institut of Chemie and Biochemie
Freie Universität Berlin
Takustr. 3, 14195 Berlin, Germany
E-mail: haag@chemie.fu-berlin.de

Prof. M. Schäfer-Korting
Institut für Pharmazie
Freie Universität Berlin
Königin-Luise-Str. 2-4, 14195 Berlin, Germany

Prof. B. Kleuser
Institut für Ernährungswissenschaft
Universität Potsdam
Arthur-Scheunert-Allee 114-116, 14558 Nuthetal, Germany

Dr. W. Li
Reference and Translation Center for Cardiac Stem Cell Therapy
Universität Rostock
Schillingallee 69, 18057 Rostock, Germany

Prof. N. Ma
Institute of Biomaterial Research
Helmholtz-Zentrum Geesthacht
Kantstraße 55, 14513 Teltow-Seehof, Germany
E-mail: nan.ma@hzg.de

DOI: 10.1002/adhm.201600212

made on tumor cell-targeted nanoparticle systems for tumor diagnosis and therapy, the development of mitochondria-targeted nanoparticle systems is still in its infancy. Therefore, it is of great importance to fabricate a mitochondria-targeted nanosystem to reach the aim of mitochondria-specific imaging for deeper understanding of tumor mitochondria, advancing early tumor diagnosis and high-performance tumor theranostics.

Up to now, some attempts have been made on developing gold nanoclusters (Au NCs),[7] quantum dot (QD),[8] magnetic nanoparticles,[8a] and carbon nanotube[9] in order to overcome the poor photostability of currently available mitochondrial dyes (such as Rhodamine, MitoTracker, JC1 dye, etc.). Among them, fluorescent nanoparticles have gained particular great interest by virtue of their excellent optical properties and low-cost, convenient, and high sensitive detection. Recently, Liu and co-workers have developed a fluorescent AuNCs@CS-TPP probe with excellent photostability and strong fluorescence emission.[7a] Jana's group has constructed a triphenylphosphonium (TPP) functionalized CdSe QDs nanoprobes for mitochondria imaging by optimized surface chemistry.[8b] These studies represent a "step forward" toward the development of stable mitochondria imaging agents. However, there are still many outstanding problems in terms of fluorescence property, safety, and versatility that required immediate solution, if a translational goal is to be achieved. The bluish or green fluorescence-emitted Au NCs and CdSe QDs suffered from interference of biological autofluorescence and limited tissue penetration depth, limiting their application. By contrast, near-infrared (NIR) fluorescence displays relatively low autofluorescence. Besides, the biocompatibility of the nanoprobes needs to be further optimized by optimizing surface modification and avoiding toxic cadmium or lead-induced toxicity. Moreover, the previously reported nanoprobes were designed only for single imaging performance, lacking versatility and flexibility for further therapeutic applications. So, a biocompatible multifunctional mitochondria-targeted NIR fluorescence nanoplatform remains highly desirable.

Previously, we have reported the synthesis of cadmium-free NIR Zn-Cu-In-S/ZnS (ZCIS/ZnS) QDs which have drawn intense attention in the field of biolabeling and tumor diagnosis owing to their low toxicity and superior optical properties.[10] Their emitted NIR fluorescence could help to reduce biological autofluorescence and background signals, facilitating precise imaging.[11] Herein, we aimed to develop a high-performance mitochondria-specific ZCIS/ZnS QDs nanoplatform via elaborate surface engineering. Polyethylene glycol (PEG) is a gold standard for improved biocompatibility, hydrophilicity, stability, and long-circulation property of nanoparticles by taking advantage of hydrogen bonding and steric stabilization effect of the ether groups.[12] However, the only one or two attachment sites limited their multifunctionalization capability. For the present study, a PEG-analogous polymer, hyperbranched polyglycerol (hPG) which has been identified to be a promising biocompatible alternative to PEG, was used to engineer ZCIS/ZnS QDs for the first time. As a highly biocompatible branched aliphatic polyether, hPG possesses not only physical properties analogous to PEG, favorable low toxicity, and low nonspecific adsorption of serum albumin but also multiple attachment sites which facilitate the attachment of other functionalities to construct flexible macromolecular assembled nanostructures.[13] It has been widely used for constructing biocompatible nanogels, biomimetic materials for targeted drug delivery, and surface antifouling. Moreover, dendritic amphiphiles with highly branched structures have been reported to be more stable micellar aggregates than linear amphiphiles.[14] All these make it an ideal candidate for the construction of versatile and multifunctional QDs nanoplatform.

In the present study, we developed an hPG-based QDs nanoplatform by incorporating near-infrared ZCIS/ZnS QDs into the assembly of our tailored hPG derivatives, amphiphilic hPG-alkyl chain (hPG-C_{12}), and hPG-TPP. The performance of the QDs@hPG-C_{12}/TPP nanoprobe for mitochondria-targeted imaging is illustrated in **Figure 1**. The introduction of TPP, an amphiphilic cation with a delocalized positive charge, could facilitate cellular uptake, effective escape from endolysosomes, and further transportation process of crossing highly dense and impermeable mitochondrial membrane.[15] And ZCIS/ZnS QDs could serve as photostable near-infrared fluorescent labels, facilitating long-term tracking of mitochondria with little biological autofluorescence and reduced background signals. The obtained QDs nanoprobe demonstrated low cytotoxicity, mitochondria-targeting ability, and superior photostability under continuous laser irradiation. Moreover, mitochondria-targeted drug-loaded QDs@hPG-C_{12}/TPP displayed enhanced tumor cell killing efficacy than nontargeted ones, indicating the great potential of QDs nanoplatform for mitochondria-acted enhanced tumor therapy. To the best of our knowledge, this is the first time to construct a mitochondria-specific NIR QDs nanoplatform with PEG-analogous hyperbranched polyglycerol. This work could open a new door to the construction of organelle-targeted multifunctional nanoplatforms for precise diagnosis and high-efficient tumor therapy.

2. Results and Discussion

2.1. Synthesis and Characterization of the hPG Derivatives

Given that high-quality ZCIS/ZnS QDs with hydrophobic 1-dodecanethiol (DDT) ligands cannot be directly used in physiological environment, hPG-based amphiphiles were hence synthesized to encapsulate the hydrophobic QDs by hydrophobic interactions. Besides, to achieve the specificity to intracellular mitochondria, a mitochondriotropic amphiphilic cation TPP that possessed a delocalized positive charge was introduced to facilitate selective accumulation of nanoparticles in mitochondria. The delocalized positive charge combines good biocompatibility with efficient membrane fusion, cellular uptake, effective escape from endosomes and lysosomes after cellular uptake, and ultimate mitochondrial targeting.[15] In order to meet the requirements for effective QDs encapsulation and mitochondria targeting, hPG derivatives including hPG-C_{12} and hPG-TPP were tailored and synthesized (**Figure 2**A). Molecular structure and GPC result of hPG we used are shown in Figure S1 (Supporting Information). Amphiphilic hPG-C_{12} was readily synthesized by the esterification reaction between terminal hydroxyl groups of hPG and lauroyl chloride. The attached long carbon chains (C_{12}) of lauric chloride (LC) acted as the hydrophobic segment of the hPG-based amphiphiles, providing the requisite amphiphilic property. Given the mitochondria targeting ability,

Adv. Healthcare Mater. 2016,
DOI: 10.1002/adhm.201600212

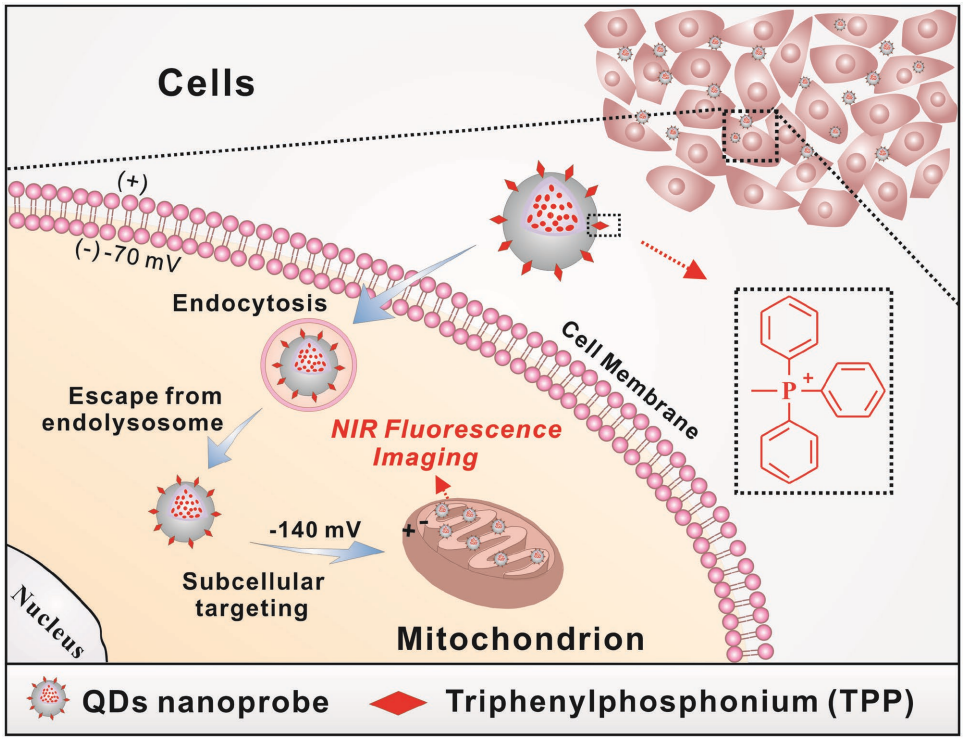

Figure 1. Schematic illustration of hyperbranched polyglycerol-based QDs@hPG-C_{12}/TPP for mitochondria-specific cell imaging.

triphenylphosphonium moieties were introduced. Owing to the low esterification reaction activity between the terminal hydroxyl of hPG and the carboxyl of (4-carboxybutyl) triphenylphosphonium bromide (CTPP) in our former trials, amine functionalized hPG (hPG-NH_2) was first prepared here by a three-step protocol. The intermediates and final hPG-NH_2 were characterized by Fourier transform infrared (FTIR) spectroscopy (Figure S2, Supporting Information). Then, hPG-TPP was prepared by conjugating CTPP to hPG-NH_2 on the basis of carbodiimide chemistry with 1-ethyl-3-(3-dimethylaminopropyl) carbodiimide hydrochloride (EDC·HCl) and *N*-hydroxysuccinimide (NHS) as the effective cross-linker. Corresponding ^{1}H NMR and FTIR spectra of the hPG derivatives are demonstrated in Figure 2B–E. Compared to the ^{1}H NMR spectrum of pure hPG in Figure 2B, the additional signals peaks at (a) 0.90 ppm, (b) at 1.30 ppm, (c) at 1.62 ppm, and (d) at 2.36 ppm in Figure 2C were attributed to H protons of lauroyl chloride, demonstrating the successful introduction of hydrophobic C_{12}. The grafting percentage of C_{12} to hydroxyl groups of hPG was about 11%, as calculated by dividing the integration of the peak areas at 0.90 ppm by that at 3.45–3.90 ppm. Meanwhile, the distinctive signal peak at 7.78–7.89 ppm derived from benzene rings suggested the success of (4-carboxybutyl) triphenylphosphonium conjugation (Figure 2D). The calculated grafting percentage of TPP to hydroxyl groups of hPG was about 5%. The FTIR spectra in Figure 2E further confirmed this by the appearance of respective characteristic absorption peak of ester bond at 1725 cm^{-1} and absorption peak of benzene from 1600 to 1400 cm^{-1}.

In general, amphiphilic polymers can spontaneously self-assemble into spherical nanostructures in water. The amphiphilic hPG-C_{12} bears hydrophilic polyglycerol and hydrophobic alkyl chains. The self-assembly and aggregation behavior triggered by hydrophobic interactions among the peripheral hydrophobic segment of alkyl chains was studied by measuring critical aggregation concentration (CAC) in deionized water with hydrophobic pyrene as a model fluorescence probe. From the fluorescence emission spectra of pyrene at various concentrations of hPG-C_{12} from 0 to 0.5 mg mL^{-1}, we could easily observe the intensity change of various peaks as the concentration increased (Figure S3, Supporting Information). The change of fluorescent intensity ratio (I_{373}/I_{384}) was plotted against the logarithm concentrations of the hPG-C_{12}. The CAC value of the hPG-C_{12} calculated by the interception of two straight lines was about 0.83 mg L^{-1}. The quite low CAC value indicated that hPG-C_{12} assemble very easily into micelle in water, reflecting its great efficiency and potential for encapsulating hydrophobic components, including small molecules and nanoparticles.

2.2. Fabrication and Characterization of the Mitochondria-Targeted QDs@hPG-C_{12}/TPP QDs Nanoprobe

In this work, high-performance hydrophobic NIR-emitted ZCIS/ZnS QDs were first prepared by using a high temperature organic solution method. Figure S4 (Supporting Information) shows a photograph of just obtained ZCIS/ZnS QDs stock solution. Different batches of QDs with tunable emission peak from 600 to 700 nm were obtained by varying the doping ratio of Zn and reaction temperature (S5). Herein, a batch of QDs (λ_{em} = 645 nm) was used. The corresponding energy dispersive spectroscopy spectrum was given in Figure S6 (Supporting Information). A simple, fast, and facile ultrasonication-induced

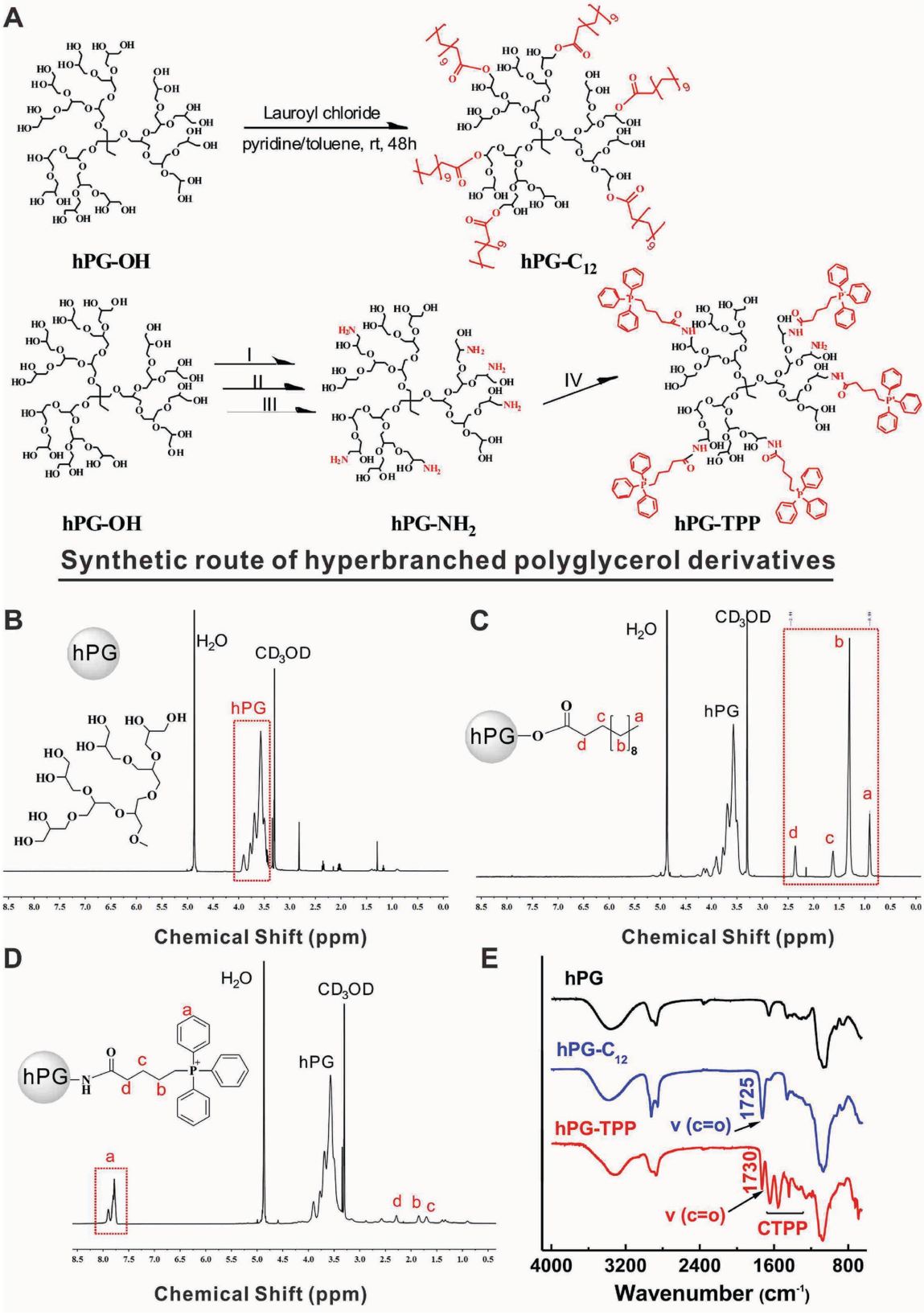

Figure 2. Synthesis and characterization of hPG derivatives. A) Synthetic route of hyperbranched polyglycerol (hPG) derivatives, amphiphilic hPG-C_{12}, and TPP-functionalized hPG-TPP. (I) MsCl, pyridine, N_2, 0 °C – rt, 24 h; (II) NaN_3, DMF, 100 °C, 12 h; (III) $P(Ph)_3$, THF/H_2O, 45 °C, 24 h; (IV) CTPP, EDC/NHS, rt, 48 h. ^{1}H NMR spectra of B) hPG, C) hPG-C_{12}, and D) hPG-TPP. E) FTIR spectra of hPG, hPG-C_{12}, and hPG-TPP.

Adv. Healthcare Mater. **2016**,
DOI: 10.1002/adhm.201600212

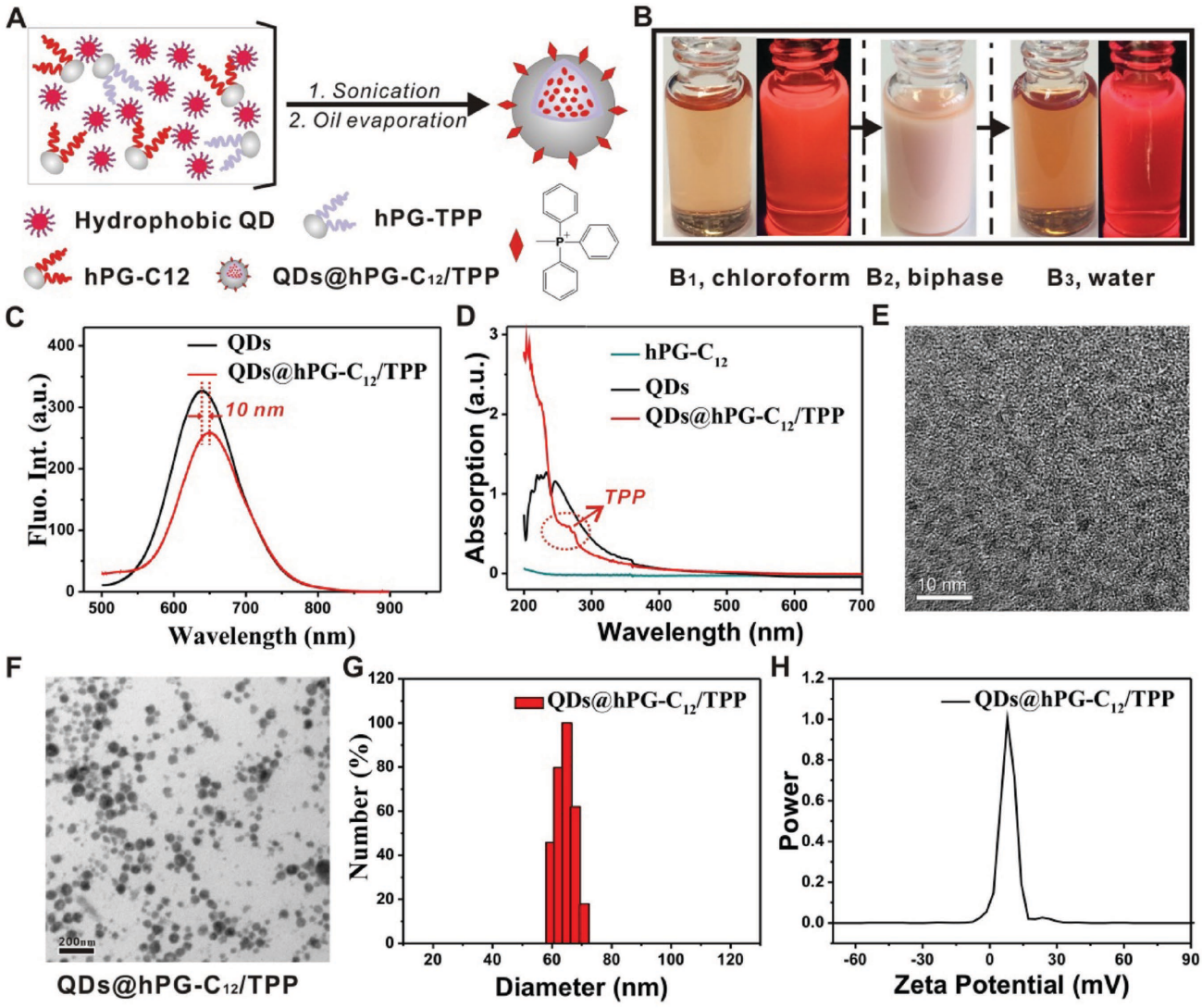

Figure 3. Preparation and characterization of the QDs nanoprobe. A) Schematic illustration of the modification procedure by an ultrasonication-based assembly method. B) The bright-field and dark-field photographs during the process of polymer modification: Hydrophobic ZCIS/ZnS QDs in chloroform (B_1), QDs emulsion system in biphase (B_2), and hydrophilic QDs@hPG-C_{12}/TPP nanoprobes in water (B_3). C) Fluorescence spectra of pure QDs and QDs@hPG-C_{12}/TPP. D) UV–vis absorbance spectra of hPG-C_{12}, QDs, and QDs@hPG-C_{12}/TPP. E,F) TEM images of pure QDs and QDs@hPG-C_{12}/TPP. G) DLS result of QDs@hPG-C_{12}/TPP. H) Zeta potential of QDs@hPG-C_{12}/TPP nanoprobes.

assembly method was employed to fabricate the QDs nanoprobes (**Figure 3**A). Upon sonication, the amphiphilic hPG derivatives assembled into micelle-like uniform spherical nanostructures which, in the presence of the hydrophobic ZCIS/ZS QDs QDs and drug molecules, spontaneously encapsulated them into the inner hydrophobic core of the micelles through strong hydrophobic interactions.

To optimize the assembly condition, we explored the influence of $m_{(hPG\text{-}C12)}/m_{(QDs)}$ ratios on the fluorescence property and hydrodynamic size of assembled QDs@hPG-C_{12} nanoprobe (Figures S7 and S8, Supporting Information). With the increase of polymer dosage in the measured range, the fluorescence intensity of obtained QDs@hPG-C_{12} nanoprobe increased while redshift distance of fluorescence emission spectrum decreased. In the meantime, Z-average size of QDs@hPG-C_{12} decreased. Taking into consideration of fluorescence property and particle size, an appropriate $m_{(hPG\text{-}C12)}/m_{(QDs)}$ ratio of 7 was employed for our later work. Characterizations of the QDs@hPG-C_{12} nanoprobes are shown in Figure S9 (Supporting Information).

To construct the mitochondria-targeted QDs nanoprobe, hPG-TPP was further added with a mass fraction of about 20%. To give a scientific and comprehensive description, visual photographs, fluorescence emission, UV–vis absorption, transmission electron microscopy (TEM) image, hydrodynamic size, zeta potential, and FTIR spectrum of the mitochondria-targeted QDs@hPG-C_{12}/TPP nanoprobe were characterized and are shown in Figure 3 and Figure S10 (Supporting Information). We could see from the photographs in Figure 3B that a homogeneous emulsion was formed under ultrasonication in the biphase system. After the oil evaporation, the QDs solution became clear and transparent, which indicated the good hydrophilicity of the obtained QDs nanoprobes. As observed

from dark-field photographs, no obvious fluorescence change occurred after the polymer modification, indicating that most of the QDs fluorescence was well retained. To further qualitatively evaluate the influence of modification process on fluorescence intensity of QDs, fluorescence spectra of pure QDs and obtained QDs nanoprobes were measured at the same QDs concentration (Figure 3C). After modification, QDs@hPG-C_{12}/TPP nanoprobes reserved about 80% of original intensity. The well-preserved fluorescence indicated the polymer layer of hPG-based derivative provided complete protection and surface passivation for the hydrophobic QDs. Compared with the UV–vis absorption spectrum of QDs@hPG-C_{12}, the appearance of characteristic absorption peak of triphenylphosphonium at 267 nm in the spectrum of QDs@hPG-C_{12}/TPP indicated successful incorporation of hPG-TPP (Figure 3D and Figure S9B, Supporting Information). As shown in Figure 3E, the original pure ZCIS/ZnS QDs were nearly monodisperse nanoparticles of ≈3 nm in size. After modification, our obtained QDs@hPG-C_{12}/TPP nanoprobes were well-dispersed uniform nanospheres with a size of 60–70 nm, and no aggregation occurred (Figure 3F). The hydrodynamic size of QDs@hPG-C_{12}/TPP nanoprobe exhibited in Figure 3G was about 65 nm which was in accordance with the size shown in TEM image. The size of QDs@hPG-C_{12} nanoprobe was slightly smaller than nontargeted ones (Figure S9C, Supporting Information). As for the zeta potential, the mitochondria-targeted QDs@hPG-C_{12}/TPP nanoprobe had a little higher zeta potential (≈7.94 mV) than the nontargeted QDs@hPG-C_{12} nanoprobe (≈3.99 mV), which was mostly induced by the residual amino groups in hPG and attached triphenylphosphonium groups (Figure 3H and Figure S9D, Supporting Information). Besides, FTIR spectrum of QDs@hPG-C_{12}/TPP nanoprobe further verified successful incorporation of hPG-TPP by the appearance of characteristic absorption peaks of benzene rings at 1600 and 1580 cm^{-1} (Figure S10, Supporting Information). All these results demonstrated that hPG derivatives-based QDs@hPG-C_{12}/TPP nanoprobe with uniform size and favorable NIR fluorescence emission was successfully fabricated by the ultrasonication-induced assembly method. It was expected that the outer polyglycerol protection layer could provide the nanoprobes with good biocompatibility, excellent stability, reduced nonspecific cellular binding, and mitochondria-specific targeting ability.

2.3. Size and Fluorescence Stability of the QDs@hPG-C_{12}/TPP Nanoprobe

The size and fluorescence stability of QDs nanoprobes is an essential issue for their further applications. In previous report, PEG chains are normally used to conjugate to polymers or onto the surfaces of particles to improve the cell survival and reduce nonspecific protein absorption of nanoparticles. For the present study, as a PEG-analogous polymer, hyperbranched polyglycerol was used to fabricate the mitochondria-targeted QDs nanoprobe. We assumed that similar structures in the repeating unit —$(OCH_2CH(CH_2OH))n$— of polyglycerol could have the same effect and offer excellent stability for the nanoprobes.

To examine the size stability of the QDs@hPG-C_{12}/TPP nanoprobe, the prepared QDs nanoprobe was gently dispersed in ultrapure H_2O, PBS buffer (0.1 M, pH 7.4), and PBS buffer supplemented with 10% fetal calf serum (FCS; PBS, 10% FCS). The particle Z-average size and polydispersity indexes (PDI) were measured by dynamic light scattering (DLS) at different incubation time using a Malvern Zetasizer. As shown in **Figure 4**A,B, the hydrodynamic size of the QDs@hPG-C_{12}/TPP nanoprobe in three kinds of solution changed little and the corresponding PDI was almost constant during 10 d of incubation. Overall, the fabricated QDs@hPG-C_{12}/TPP nanoprobe with hPG-based amphiphiles exhibited excellent size stability. This stability was probably provided by the supermolecular assembly structures of highly branched hPG-based derivatives.[14a]

As for a fluorescence nanoprobe, fluorescence stability in biological fluids is of vital importance for its use in accurate quantitative imaging analysis and in tumor diagnostics. In general, the fluorescence could be easily quenched if the surface coating is not complete and compact enough to completely isolate the hydrophobic QDs from water environment. Herein, fluorescence intensities of the QDs@hPG-C_{12}/TPP nanoprobes in PBS with 10% FCS at 37 °C were investigated. As demonstrated in Figure 4C, the nanoprobes kept good fluorescence in the measured 10 d and showed no obvious change in fluorescence intensity, indicating excellent fluorescence stability.

2.4. In Vitro Cytotoxicity

The cytotoxicity of the amphiphilic hPG-C_{12}, QDs@hPG-C_{12}, and QDs@hPG-C_{12}/TPP nanoprobes against HeLa cells was assessed by using 3-(4,5-dimethylthiazol-2-yl)-2,5-diphenyl tetrazolium bromide (MTT) assay. The viability of cells exposed to different concentrations (12.5, 25, 50, 100, 200, and 400 μg mL^{-1}) of three samples for 24 h is shown in Figure 4D. With an increase in concentration of QDs@hPG-C_{12} and QDs@hPG-C_{12}/TPP nanoprobes from 25 to 400 μg mL^{-1}, the cell survival decreased slightly. At the concentration of 400 μg mL^{-1}, the cell survivals of HeLa cells incubated with the three samples were all above 80%. The hPG-based amphiphilic hPG-C_{12}, QDs@hPG-C_{12} nanoprobes, and the mitochondria-targeted QDs@hPG-C_{12}/TPP nanoprobes all had a low cytotoxicity in the measured concentration range. Although QDs@hPG-C_{12}/TPP nanoprobe possessed a slightly higher zeta potential value than QDs@hPG-C_{12} nanoprobe, we did not observe more toxic effects of this formulation. In particular, the viability of cells incubated with hPG-C_{12} was always above 100%. The hPG-based amphiphilic polymer hPG-C_{12} did not cause any cytotoxicity against HeLa cells under the concentration of 400 mg mL^{-1}, suggesting low in vitro cytotoxicity. As a biocompatible branched aliphatic polyether analogous to those of PEG, hPG-based amphiphilic hPG-C_{12} had great potential in the field of constructing biocompatible nanoplatforms via modifying various hydrophobic nanoparticles.

2.5. Cell Imaging and Mitochondria-Targeted Subcellular Imaging of the QDs@hPG-C_{12}/TPP Nanoprobe

To investigate the cell uptake and fluorescence imaging performance of the mitochondria-targeted QDs@hPG-C_{12}/TPP

Adv. Healthcare Mater. 2016,
DOI: 10.1002/adhm.201600212

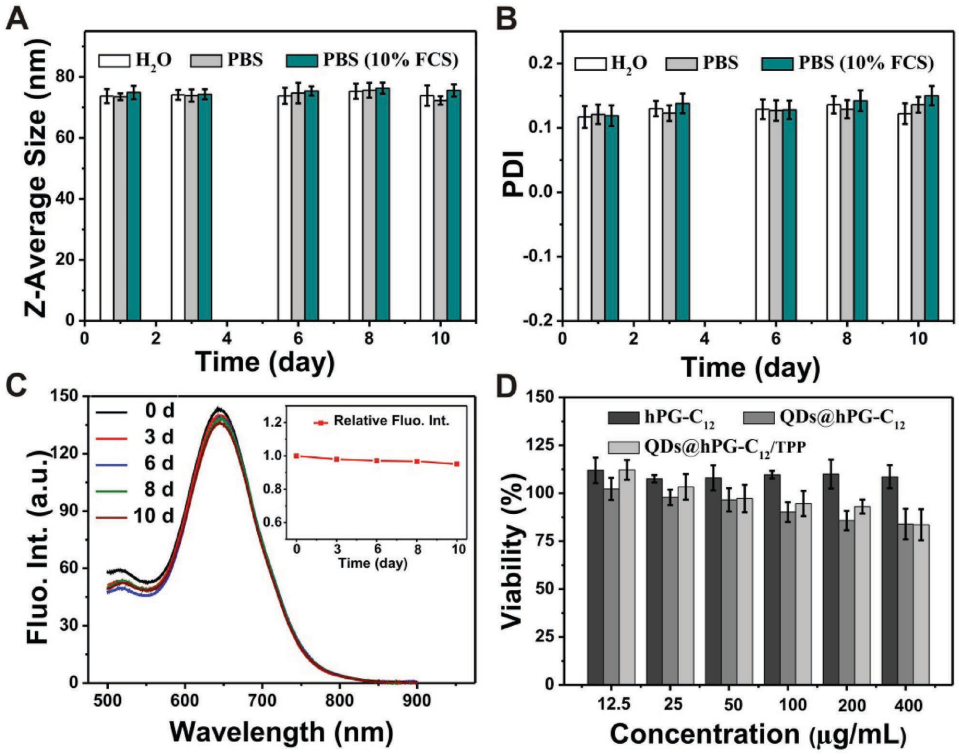

Figure 4. Stability and cytotoxicity of the QDs nanoprobes. A,B) Z-average size and polydispersity index (PDI) stability of QDs@hPG-C_{12}/TPP in doubly distilled water, PBS buffer (pH 7.4), and PBS buffer (pH 7.4) supplemented with 10% FCS. C) Fluorescence stability of QDs@hPG-C_{12}/TPP in PBS buffer (pH 7.4) supplemented with 10% FCS. D) In vitro cytotoxicity studies of hPG-C_{12}, QDs@hPG-C_{12}, and QDs@hPG-C_{12}/TPP using the MTT assay in HeLa cells.

nanoprobes, HeLa cells were used as a model and nontargeted QDs@hPG-C_{12}/TPP nanoprobes as a control. To test the temporal evolutions, HeLa cells were exposed to QDs nanoprobes for different incubation time periods (0.5, 1.5, and 3 h). As shown in **Figure 5**A and Figure S11 (Supporting Information), the fluorescence intensity of QDs in HeLa cells increased with time, which indicated an ongoing cell uptake. By contrast, little nontargeted QDs@hPG-C_{12} nanoprobes were internalized by HeLa cells after incubation for 3 h on account of the extremely low nonspecific absorption of the hyperbranched polyglycerol-based surface coating. The mitochondria-targeted QDs@hPG-C_{12}/TPP nanoprobes demonstrated a significantly enhanced cell uptake than nontargeted ones. It was mentioned in previous report that delocalized positive charge in TPP could promote membrane fusion and cellular uptake.[16] Therefore, the introduced triphenylphosphonium moieties effectively promoted the cell uptake of the nanoprobes as a lipophilic cation along with the residual amino groups on hPG. Taken together, the hPG-based polymer coating endowed the nanoprobes excellent biocompatibility and low cytotoxicity, while the introduction of TPP moieties significantly promoted the cell uptake of the QDs nanoprobes. Meanwhile, the flow cytometry analysis further verified the enhanced cell uptake of TPP-decorated QDs@hPG-C_{12}/TPP nanoprobe than nontargeted ones (Figure 5B). The change of mean fluorescence intensity of M area over time is demonstrated in Figure 5C. As time prolonged, the mean fluorescence intensity of M2 area increased significantly from 37.97 to 131.77 in the group of QDs@hPG-C_{12}/TPP nanoprobe, while it remained consistently at a low value (<36) in the group of QDs@hPG-C_{12} nanoprobe.

To test the feasibility of QDs@hPG-C_{12}/TPP nanoprobes for mitochondria-specific imaging, confocal fluorescence images of HeLa cells treated with QDs@hPG-C_{12}/TPP were taken by Leica TCS SP5 Confocal Laser Scanning Microscope (CLSM). To avoid mutual fluorescence interference of QDs and mitochondrial staining dye, MitoTracker with excitation wavelength of 644 nm from Invitrogen was employed for the co-localization study. To distinguish colors of QDs and MitoTracker, Mito Tracker and QDs were set as red and green, respectively. **Figure 6**A shows confocal images of untreated HeLa cells stained with only Mito Tracker as negative control. No fluorescence in the QDs emission channel was observed in untreated HeLa cells, which suggested that excitation light of 633 nm had no interference with QDs channel. Further, confocal images of HeLa cells treated separately with nontargeted QDs@hPG-C_{12} and targeted QDs@hPG-C_{12}/TPP are shown in Figure 6B,C. As shown in Figure 6B, there was almost no QDs fluorescence in the HeLa cells after incubation with nontargeted QDs@hPG-C_{12} for 1.5 h. This was caused by the weak endocytosis of QDs@hPG-C_{12} proved in cell uptake experiment. The outer polyglycerol makes it had a quite low cell adsorption and weak uptake. It was previously reported that hPG could reduce nonspecific adsorption to

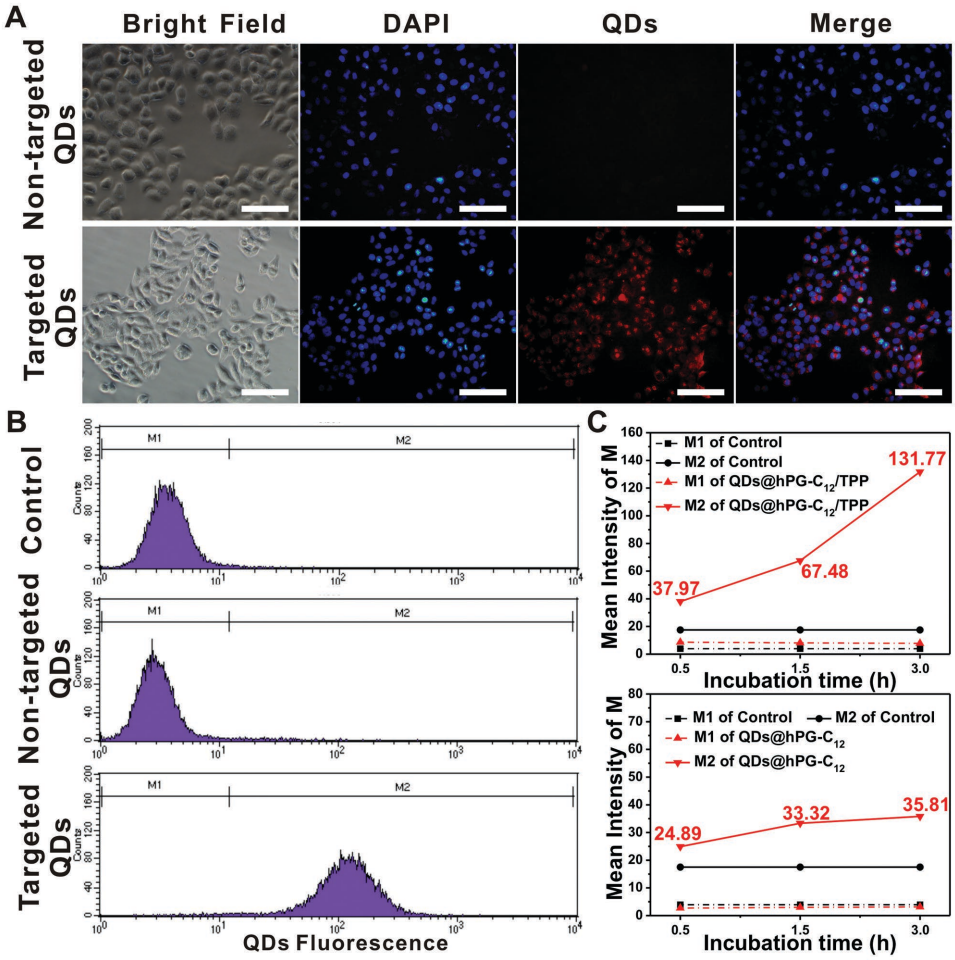

Figure 5. Cellular imaging of the QDs nanoprobes. A) Fluorescent images and B) flow cytometry analysis of HeLa cells incubated separately with nontargeted QDs@hPG-C_{12} and mitochondria-targeted QDs@hPG-C_{12}/TPP nanoprobes at 37 °C for 3 h. Scale bar represents 100 μm. C) The change of mean fluorescence intensity of M area in (B) over incubation time. The HeLa cells without any treatment were used as control.

nanoparticles by blocking protein-binding sites and creating a thermodynamic barrier to protein diffusion. By contrast, QDs@hPG-C_{12}/TPP could be effectively endocytosed into HeLa cells under the same condition and then selectively and specifically accumulate into intracellular mitochondria (Figure 6C). The selectivity was originated from the specific conjugation of TPP with mitochondria, which had been reported in previous work.[18] As a lipophilic cation with three phenyl groups and delocalized positive charge, triphenylphosphonium could ensure effective escape from endosomes and lysosomes facilitate further transportation process of crossing the impermeable mitochondrial membrane. Based on the above analysis, mitochondria-targeted QDs@hPG-C_{12}/TPP nanoprobe was successfully fabricated. What's more, the near-infrared fluorescence emission could effectively avoid interference of biological autofluorescence and reduce background signals. In general, our tailor-designed ZCIS/ZnS QDs nanoprobe with near infrared fluorescence emission is an ideal fluorescent nanoparticle for mitochondria-specific labeling, imaging, and tracking in tumor cells.

2.6. Photostability of QDs@hPG-C_{12}/TPP Nanoprobe

Photostability is very critical for the development of fluorescent probes and their applications for long-term labeling and tracking. To investigate the photostability of our constructed QDs@hPG-C_{12}/TPP nanoprobe under irradiation, HeLa cells treated with QDs@hPG-C_{12}/TPP and MitoTracker were irradiated by laser confocal microscope with excitation at 453 nm (50% laser power) and 633 nm (15% laser power), respectively. As shown in **Figure 7**B, there was almost no change in the fluorescence intensity of QDs@hPG-C_{12}/TPP nanoprobes in HeLa cells after 8 min of irradiation. However, the fluorescence intensity of the MitoTracker decreased gradually as irradiation time prolonged, indicating that the commercially available MitoTracker suffered from poor photostability (Figure 7A). Moreover, the mean fluorescence intensities of selected regions of interest (ROI) at different scanning time were analyzed by CLSM and are shown in Figure 7B. It was easily observed that the fluorescence of MitoTracker gradually bleached under irradiation while that of QDs nanoprobe remained unchanged,

Adv. Healthcare Mater. **2016**,
DOI: 10.1002/adhm.201600212

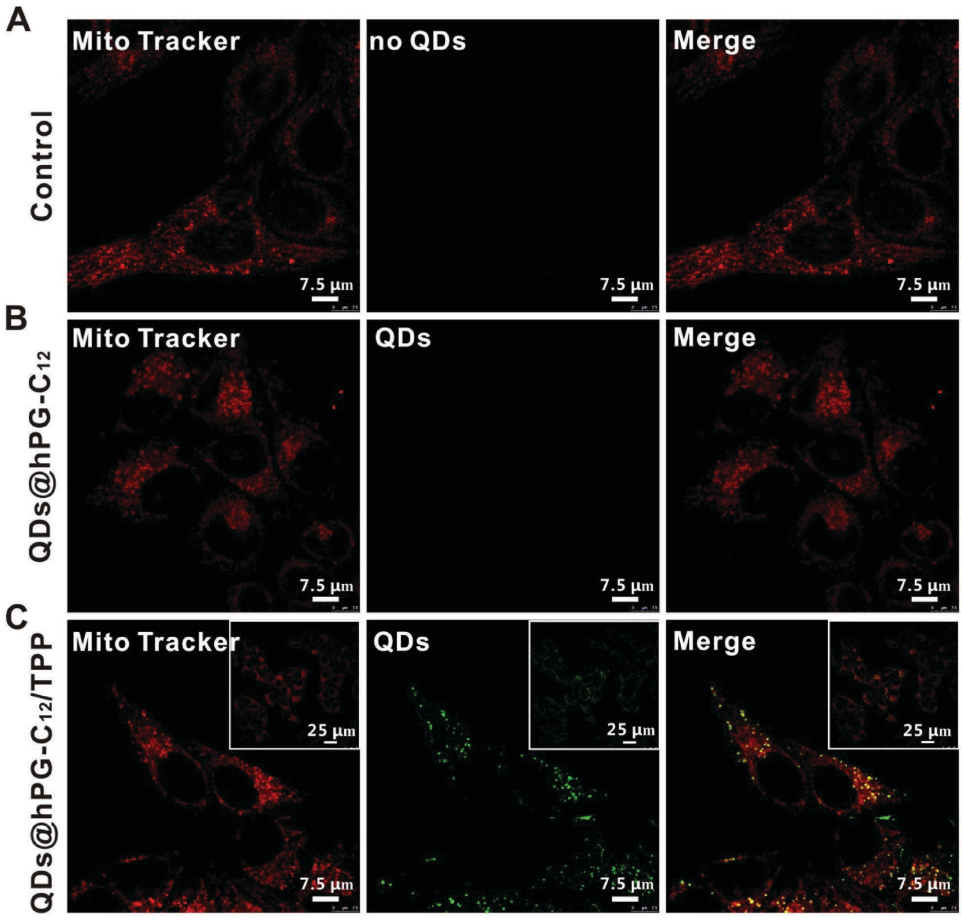

Figure 6. Subcellular localization of QDs@hPG-C_{12}/TPP nanoprobes by confocal fluorescent images. A) Untreated HeLa cells stained with Mito Tracker Deep Red FM. B) HeLa cells treated with QDs@hPG-C_{12} and Mito Tracker. C) HeLa cells treated with QDs@hPG-C_{12}/TPP and Mito Tracker. The insets show broader field of view. Mito Tracker and QDs were set as red and green, respectively. Excitation wavelength: 453 nm for QDs and 633 nm for Mito Tracker.

from which we could further confirm that our constructed QDs@hPG-C_{12}/TPP nanoprobes possessed excellent photostability and could serve as an alternative to currently commercially available mitochondria dyes. More importantly, the bright near-infrared fluorescence emission without photobleaching and mitochondria targeting ability make it a very promising nanoprobe for long-term and sensitive mitochondria imaging in living cells and mitochondria-related tumor diagnosis in vivo.

2.7. Application of Drug-Loaded QDs@hPG-C_{12}/TPP for Enhanced Chemotherapy In Vitro

Compared with previously reported nanoprobe with single mitochondria imaging performance, our constructed flexible QDs@hPG-C_{12}/TPP could be expanded as a versatile nanoplatform for therapeutic applications by further loading drugs, making it a promising cancer theranostic agent. Owing to the higher susceptibility of mitochondria in cancer cells to mitochondria-acting drugs, mitochondria have recently become interesting targets for tumor therapy. Targeted delivery of drugs to intracellular organelles of interest could be highly effective in maximizing the drug effects and enhancing treatment efficacy.[18] To further prove the mitochondria-targeted ability and examine the versatility of this mitochondria-targeted system in cancer chemotherapy, anticancer drugs, doxorubicin (DOX) and betulinic acid (BA), were separately loaded to construct drug-loaded nanomedicine. The preparation of drug-loaded QDs@hPG-C_{12}/TPP nanomedicine for precisely image-guided mitochondria-acted enhanced tumor chemotherapy is illustrated in Figure S12 (Supporting Information). The inhibitory effect of the drug-loaded QDs@hPG-C_{12}/TPP nanomedicine on the proliferation of HeLa cells was evaluated by the MTT assay. The pure drug and nontargeted drug-loaded nanomedicine were used as control. As shown in Figure S13 (Supporting Information), at the same drug concentration of 5 and 10 μg mL^{-1}, mitochondria-targeted DOX-loaded QDs@hPG-C_{12}/TPP nanomedicine exhibited obviously higher inhibited proliferation effect on HeLa cells than nontargeted DOX-loaded QDs@hPG-C_{12} nanoprobes. The same phenomenon occurred when BA was loaded. All these mitochondria-targeted nanomedicine exhibited higher

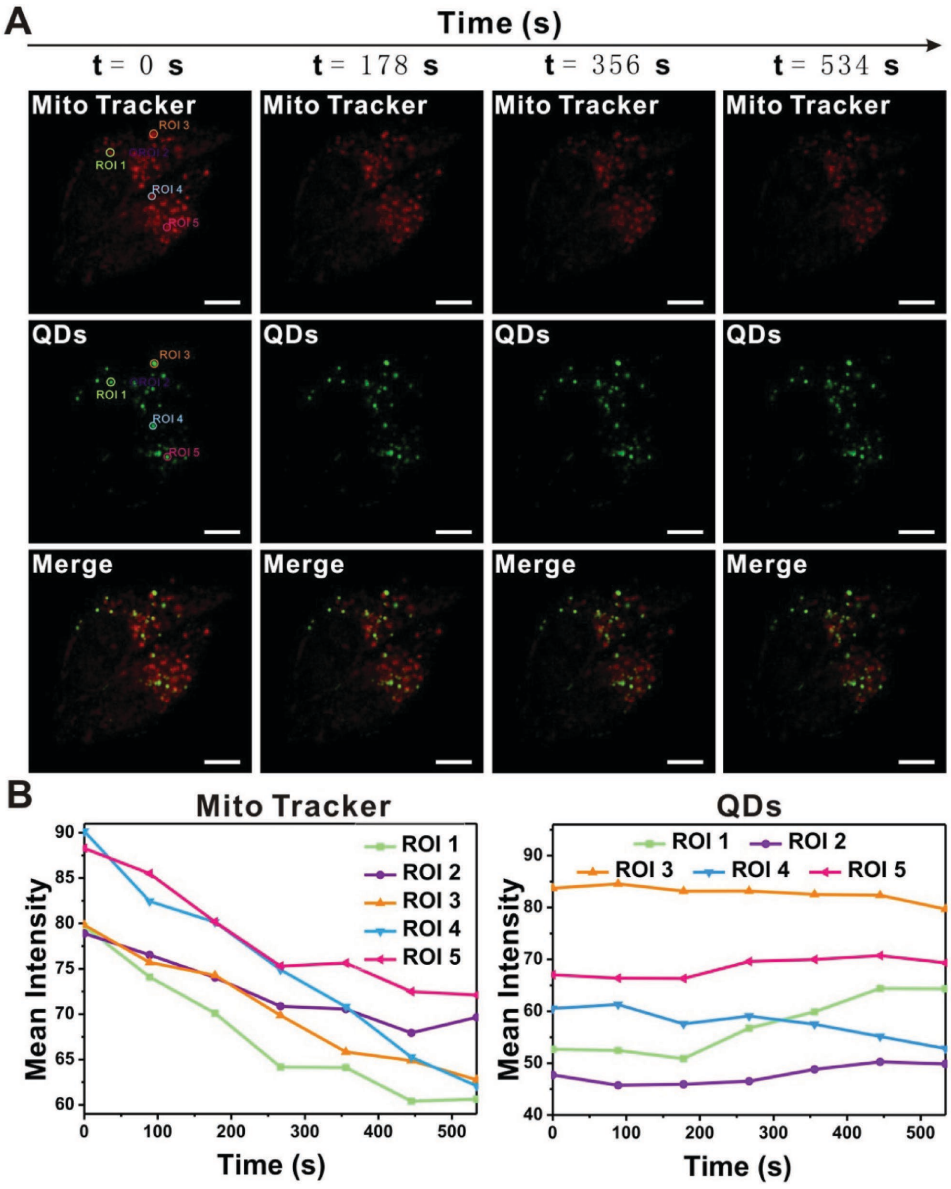

Figure 7. Photostability study of QDs@hPG-C_{12}/TPP nanoprobe. A) Confocal fluorescent images of HeLa cells stained with QDs@hPG-C_{12}/TPP and Mito Tracker Deep Red FM with increasing scanning time (0–8 min). Mito Tracker and QDs were set as red and green, respectively. Excitation wavelength: 453 nm (50% laser power) for QDs and 633 nm (20% laser power) for Mito Tracker Deep Red FM. Scale bar represents 7.5 μm. B) The change of mean fluorescence intensity of Mito Tracker and QDs in the selected region of interest (ROI) in (A) over time.

anticancer activity than the nontargeted groups. Therefore, enhanced tumor cell killing efficacy was achieved with TPP-functionalized QDs nanomedicine via specifically delivering drugs to mitochondria in our present work. The versatile drug-loaded QDs nanoplatform could realize precisely image-guided mitochondria-acted enhanced chemotherapy efficacy. There was only a preliminary exploration in our present work, and detailed optimization of this nanoplatform should be further carried out. Moreover, it has been reported that mitochondrial-targeted drug therapy could help to overcome multidrug resistance in tumor chemotherapy, representing a promising approach to eradicate chemotherapy-refractory cancer cells. Therefore, our constructed versatile hyperbranched polyglycerol-based QDs nanoplatform has great potential for enhanced high-efficiency tumor theranostic. This nanoplatform could also be employed for targeted delivery of other mitochondria-acting drug such as lonidamine and α-tocopheryl succinate to mitochondria of cells. Further explorations of its blood circulation stability, imaging ability, and anticancer effect in vivo need to be done before their translation to the clinic.

3. Conclusions

In conclusion, a highly photostable hyperbranched polyglycerol-based NIR QDs nanoplatform was successfully constructed

Adv. Healthcare Mater. **2016**,
DOI: 10.1002/adhm.201600212

and utilized for mitochondria-specific imaging and enhanced chemotherapy efficacy in HeLa cells. The QDs@hPG-C_{12}/TPP nanoprobe was featured by uniform size, NIR fluorescence emission, good stability, low cytotoxicity, mitochondria-targeting ability, and superior photostability compared with commercial deep-red mitochondria dyes under continuous laser irradiation. Besides, drug-loaded QDs@hPG-C_{12}/TPP displayed an obviously enhanced tumor cell killing efficacy than nontargeted ones. All these excellent advantages make this QDs@hPG-C_{12}/TPP nanoplatform a promising candidate for long-term real-time mitochondria labeling and tracking. The near-infrared photostable fluorescence and cadmium and lead-free composition provide this nanoprobe more possibilities for clinical and translational applications. Moreover, it has great potential in the delivery of mitochondria-acting drugs for image-guided high-efficient treatment of tumor and other mitochondria-related diseases. We hope this work could open the door to the construction of multifunctional organelle-targeted theranostic nanoplatforms.

4. Experimental Section

Materials: hPG (M_n = 11.1 kg mol^{-1}, M_w = 17.9 kg mol^{-1}, PDI = 1.61) was synthesized according to a previously published procedure.[16] Sulfur (S, 99.9%), indium(III) acetate ($In(Ac)_3$, 99.99%), copper(I) iodide (CuI, 99.999%), zinc acetate dehydrate ($Zn(Ac)_2.2H_2O$, reagent grade), oleic acid (OA, 90%), oleylamine (97%), DDT (98%), 1-octadecene (ODE, 90%), LC (≥99.8%), CTPP, pyridine (dry, ≥99.9%), toluene (dry), and dimethylformamide (DMF, dry) were purchased from Sigma-Aldrich (Germany). Methanesulfonyl chloride (MsCl), triethylamine (Et_3N), sodium azide (NaN_3), triphenylphosphine, succinic anhydride (99.5%), NHS, EDC·HCl, and MTT were procured from Acros (Germany) or Fluka (Germany). MitoTracker Deep Red FM was purchased from Invitrogen (German). All other reagents and solvents without statement were of reagent or HPLC grade and used without further treatment. For cell culture experiments, HeLa cells cultured in Dulbecco's Modified Eagle Medium (DMEM, supplemented with 1% penicillin streptomycin antibiotics, 10% fetal bovine serum, FBS) at 37 °C under a 5% CO_2 atmosphere were used. Ultrapure water (Millipore Inc., Bedford, MA) was used in all experiments and for preparation of all samples.

Preparation of ZCIS/ZnS QDs: Different batches of ZCIS/ZnS QDs with emission peak from 600 to 700 nm were prepared as previously described.[10a,b] In brief, $Zn(Ac)_2$ (0.05 mmol), CuI (0.1 mmol), $In(Ac)_3$ (0.2 mmol), DDT (1 mL), OA (500 µL), and ODE (10 mL) were mixed under stirring in a 50 mL round-bottom flask and heated to 120 °C until a clear solution was formed. The reaction system was degassed for 20 min, backfilled with Ar, subsequently heated to 230 °C followed by injection of 1.0 mL of sulfur precursor (0.3 M in ODE/oleylamine, the ratio is 2/1), and finally kept at the temperature for 30 min for the growth of ZCIS/ZnS QDs core. In order to improve the fluorescence intensity of the QDs, 2 mL of $Zn(Ac)_2$ stock solution (0.2 M in ODE/oleylamine, the ratio is 1/1) was injected into the reaction mixture in four batches with a time interval of 15 min for the deposition of ZnS shell. The ZCIS/ZnS QDs were collected by adding acetone and centrifugation (9000 rpm, 10 min), purified two times again with chloroform/acetone mixture, and finally dispersed in chloroform and stored at 4 °C for further use.

Synthesis of Hyperbranched Polyglycerol-C_{12} (hPG-C_{12}) and Polyglycerol-hPG-TPP: The hyperbranched polyglycerol was prepared by a one-step ring-opening anionic polymerization as previously reported.[20]

Synthesis of hPG-C_{12}: The amphiphilic hPG-C_{12} was prepared via an acyl chloride esterification method. Lauroyl chloride (328 µL, 1.42 mmol) dissolved in 6 mL of toluene was added dropwise to a solution of dried hyperbranched polyglycerol (1 g, 13.5 mmol —OH) in 30 mL of pyridine. After stirring for 48 h, most of the solvents were removed by rotary evaporation. The polymer was then subjected to dialysis against chloroform and methanol to remove toluene, pyridine, and free lauroyl chloride, and finally dried under vacuum to obtain dry products with a yield of 90%. Determined by the ^{1}HNMR, the grafting degree of C_{12} was about 10%.

Synthesis of hPG-TPP: Due to the large steric hindrance of triphenylphosphonium groups, esterification of the terminal hydroxyl of hPG and the carboxyl of CTPP is very low. So amine functionalized hPG (hPG-amine) was first prepared here to increase the grafting degree of CTPP by a three-step protocol according to the previously reported method.[18] In brief, the OH groups of polyglycerol was first conversed into mesyl (Ms) groups by reacting with methanesulfonyl chloride, conversed into azide (N_3) functionalities by reacting with NaN_3, and finally reduced to primary amino (NH_2) groups by using triphenylphosphine as a reducing agent. hPG-amine with an amination degree of 10% was readily prepared and employed in our present work.

hPG-TPP was prepared on the basis of carbodiimide chemistry with EDC·HCl and NHS as the effective cross-linker. Typical procedure was conducted as follows: Briefly, hPG-amine (300.0 mg, 4.0 mmol of primary hydroxyl and amine groups, 9:1) and CTPP (215.6 mg, 0.5 mmol carboxyl groups) were dissolved in 15 mL of anhydrous DMF, followed by successively adding NHS (139.9 mg, 1.2 mmol) and EDC·HCl (232.5 mg, 1.2 mmol), which were 2.4 times the theoretical amount to ensure the conjugation efficiency. The mixture was kept at room temperature and protected from light under vigorous stirring for 24 h, and then subjected to dialysis against methanol (MWCO = 2000) to remove the byproduct and free CTPP, and finally dried under vacuum to obtain dry products. Calculated from ^{1}HNMR, the real grafting ratio of CTPP is about 5%.

Determination of CAC: The amphiphilic hPG-C_{12} bears hydrophilic polyglycerol and hydrophobic alkyl chains. Herein, their self-assembly behavior, triggered by hydrophobic interactions among peripheral hydrophobic segment of alkyl chains, was studied by measuring CAC value with hydrophobic pyrene as a model fluorescence probe. The concentration of pyrene was set as 6.0×10^{-7} M. The fluorescence emission spectra of pyrene when excited by an ultraviolet light at 338 nm were measured at various concentrations of polymer from 0 to 0.5 mg mL^{-1}. The emission intensities at 373 and 384 nm were recorded.

Preparation of Mitochondria-Targeted QDs@hPG-C_{12}/TPP and Drug-Loaded QDs@hPG-C_{12}/TPP: The QDs@hPG-C_{12}/TPP nanoprobe was prepared via a previously reported ultrasonication-induced assembly method with minor modifications.[10b] In brief, 500 µL of oil solution (6.0 mg mL^{-1} of QDs and 6.0 mg of hPG-TPP in chloroform) was injected dropwise into 3 mL of cold hPG-C_{12} solution (5.0 mg mL^{-1} in water) under pulsed ultrasonication every 7 s for a duration of 3 s at 100–200 W for 8 min to form an emulsion. The solution was then evaporated to remove the residual chloroform until it was completely clear. The clear QDs@hPG-C_{12} solution was further purified by centrifugation at 20 000 g for 20 min and washed to remove residual polymer and finally stored at 4 °C away from light. Herein, an ultrasonic cell crushing instrument with an ultrasonic booster (JY92-IID, Ningbo Scientz Biotechnology Co., LTD) was used.

The preparation of mitochondria-targeted QDs@hPG-C_{12} and drug-loaded QDs@hPG-C_{12}/TPP was conducted in a similar way, except that no hPG-TPP or extra drugs were added in the chloroform.

Size and Fluorescence Stability of QDs@hPG-C_{12}/TPP: The size and fluorescence stability of nanoprobes in aqueous media are both very critical for their application for long-lime real imaging. In this work, to investigate whether the surface modification with hPG-based derivatives could provide a good stability, the size and fluorescence changes against time were monitored. The prepared mitochondria-targeted QDs@hPG-C_{12}/TPP nanoprobe solution was gently mixed ultrapure H_2O, PBS buffer (0.1 M, pH 7.4), and PBS buffer supplemented with 10% FCS (PBS, 10% FCS), respectively. After different periods of incubation time, their average size was monitored by DLS using a Malvern Zetasizer. Every sample was measured at least three times and averaged. Besides, the fluorescent stability of QDs@hPG-C_{12}/TPP nanoprobes was further

investigated. The fabricated nanoprobe was incubated in PBS buffer (0.01 M, pH = 7.4) supplemented with 10% FCS, and its fluorescence emission intensity at different incubation time was measured by fluorescence spectrophotometer.

Cytotoxicity, Cell Uptake, and Intracellular Studies

Cell culture: Human cervical cancer HeLa cell line was used for cytotoxicity, cellular uptake, and intracellular studies as a model. The untreated cells served as negative control. The HeLa cell line was routinely cultured in DMEM (supplemented with 10% fetal bovine serum and 1% penicillin streptomycin antibiotics), incubated at 37 °C in a humidified atmosphere with 5% CO_2, and split 1:4 three times a week.

Cytotoxicity assays: Cytotoxicity of the amphiphilic polymer hPG-C_{12}, QDs@hPG-C_{12}, and QDs@hPG-C_{12}/TPP nanoprobes was evaluated by using the MTT assay. HeLa cells were seeded in a 96-well plate at a density of 5×10^3 cells per well in Dulbecco's Modified Eagle Medium and incubated at 37 °C in a humidified atmosphere with 5% CO_2 for 24 h. The prepared samples were diluted in DMEM at serial concentrations of 12.5, 25, 50, 100, 200, and 400 μg mL^{-1} and then added to replace the original culture medium. After a further incubation for 24 h, 20 μL of MTT stock solution (5 mg mL^{-1} in H_2O) was added per well for an additional 4 h, and then replaced by 100 μL of DMSO each well for 10 min under shaking. The UV absorbance of MTT at 570 nm was measured by a microplate reader. Cell viability was calculated by comparing the absorbance of cells treated with samples to that of nontreated cells.

Cell uptake of QDs@hPG-C_{12}/TPP nanoprobes measured by fluorescence microscopy and flow cytometry: The cell uptake and fluorescence imaging of the mitochondria-targeted QDs@hPG-C_{12}/TPP nanoprobes and nontargeted QDs@hPG-C_{12} nanoprobes were observed by fluorescence microscope with HeLa cells as a model. HeLa cells were seeded into a 24-well plate at a density of 5.0×10^4 to 1.0×10^5 cells per well and incubated in DMEM medium supplemented with 1% penicillin/streptomycin and 10% FBS under a 5% CO_2 atmosphere at 37 °C. After incubation for 24 h, about 30 μL of QDs@hPG-C_{12} and QDs@hPG-C_{12}/TPP nanoprobe solutions were, respectively, added to the culture medium. After further incubation for predetermined time, the medium was removed and the cells were washed three times with PBS buffer. For cellular fluorescence imaging study, the cells were fixed with 4% paraformaldehyde for 20 min and then stained with 200 μL of DAPI solution (1 μg mL^{-1}) for 20 min for nucleus staining. Finally, the cells were washed twice with PBS buffer and subjected to fluorescence microscopy. In addition, flow cytometry was further used to quantify the cellular uptake of the QDs@hPG-C_{12} and QDs@hPG-C_{12}/TPP nanoprobes with a flow cytometer on a FACSCalibur (BD Biosciences).

Intracellular mitochondria-specific imaging measured by confocal laser scanning microscopy: HeLa cells were seeded into a 24-well plate with glass slides on bottom for 24 h. Next, nontargeted QDs@hPG-C_{12} and mitochondria-targeted QDs@hPG-C_{12}/TPP nanoprobe solutions (100–200 μg mL^{-1}) were, respectively, added to the culture medium for 1.5 h for the attachment of nanoprobes with the cell membrane. Then, the culture medium was replaced by fresh media and incubated for another 6 h for particle intracellular localization. For the co-localization study, the cells were further stained with MitoTracker Deep Red FM (50×10^{-9} M) at 37 °C for 30 min, washed three times with PBS buffer, and finally imaged under Leica TCS SP5 CLSM.

Photostability of QDs@hPG-C_{12}/TPP: To investigate the photostability of the QDs@hPG-C_{12}/TPP nanoprobe, HeLa cells treated with QDs@hPG-C_{12}/TPP nanoprobe and MitoTracker were imaged by Leica TCS SP5 Confocal Microscope. QDs@hPG-C_{12}/TPP nanoprobes were excited at 453 nm (50% laser power) and the fluorescence emission was collected from 550 to 700 nm. The MitoTracker was excited at 633 nm (15% laser power) and fluorescence emission was collected from 650 to 750 nm.

Application of drug-loaded QDs@hPG-C_{12}/TPP for enhanced chemotherapy in vitro: Two anticancer drugs, DOX and BA, were separately loaded inside nontargeted QDs@hPG-C_{12} and mitochondria-targeted QDs@hPG-C_{12}/TPP nanoprobes to construct drug-loaded nanomedicine to evaluate the therapeutic efficiency. The MTT assay was used to assess the cell viability. The cells were treated with 5 and 10 μg mL^{-1} of pure drug and the nanomedicine at equivalent drug concentration at 37 °C for 24 h.

Supporting Information

Supporting Information is available from the Wiley Online Library or from the author.

Acknowledgements

C.D. and Z.L. contributed equally to this work. The authors gratefully acknowledge the National Natural Science Foundation of China (Grant Nos. 51373117, 51573128, and 51303126), the Key Project of Tianjin Natural Science Foundation (Grant Nos. 13JCZDJC33200 and 15JCQNJC03100), the National High Technology Program of China (Grant No. 2012AA022603), the Doctoral Base Foundation of the Educational Ministry of China (Grant No. 20120032110027), and SFB 1112 for financial support.

Received: February 26, 2016
Revised: March 29, 2016
Published online:

[1] S. Fulda, L. Galluzzi, G. Kroemer, *Nat. Rev. Drug Discovery* **2010**, *9*, 447.
[2] L. Rajendran, H.-J. Knölker, K. Simons, *Nat. Rev. Drug Discovery* **2010**, *9*, 29.
[3] a) J. A. Canter, A. R. Kallianpur, F. F. Parl, R. C. Millikan, *Cancer Res.* **2005**, *65*, 8028; b) J. A. Petros, A. K. Baumann, E. Ruiz-Pesini, M. B. Amin, C. Q. Sun, J. Hall, S. Lim, M. M. Issa, W. D. Flanders, S. H. Hosseini, *Proc. Natl. Acad. Sci. USA* **2005**, *102*, 719.
[4] V. Gogvadze, S. Orrenius, B. Zhivotovsky, *Trends Cell Biol.* **2008**, *18*, 165.
[5] a) S. Marrache, R. K. Pathak, S. Dhar, *Proc. Natl. Acad. Sci. USA* **2014**, *111*, 10444; b) G. R. Chamberlain, D. V. Tulumello, S. O. Kelley, *ACS Chem. Biol.* **2013**, *8*, 1389; c) J. L. Hickey, R. A. Ruhayel, P. J. Barnard, M. V. Baker, S. J. Berners-Price, A. Filipovska, *J. Am. Chem. Soc.* **2008**, *130*, 12570; d) R. K. Pathak, S. Marrache, D. A. Harn, S. Dhar, *ACS Chem. Biol.* **2014**, *9*, 1178.
[6] A. Mallick, P. More, S. Ghosh, R. Chippalkatti, B. A. Chopade, M. Lahiri, S. Basu, *ACS Appl. Mater. Interfaces* **2015**, *7*, 7584.
[7] a) Q. Zhuang, H. Jia, L. Du, Y. Li, Z. Chen, S. Huang, Y. Liu, *Biosens. Bioelectron.* **2014**, *55*, 76; b) L. Wang, Y. Liu, W. Li, X. Jiang, Y. Ji, X. Wu, L. Xu, Y. Qiu, K. Zhao, T. Wei, *Nano Lett.* **2010**, *11*, 772.
[8] a) A. Chakraborty, N. R. Jana, *J. Phys. Chem. C* **2015**, *119*, 2888; b) A. M. Derfus, W. C. Chan, S. N. Bhatia, *Adv. Mater.* **2004**, *16*, 961.
[9] a) F. Zhou, S. Wu, Y. Yuan, W. R. Chen, D. Xing, *Small* **2012**, *8*, 1543; b) F. Zhou, S. Wu, B. Wu, W. R. Chen, D. Xing, *Small* **2011**, *7*, 2727.
[10] a) W. Guo, *Theranostics* **2013**, *3*, 99; b) C. Dong, Z. Liu, L. Zhang, W. Guo, X. Li, J. Liu, H. Wang, J. Chang, *ACS Appl. Mater. Interfaces* **2015**, *7*, 7566; c) Z. Liu, N. Chen, C. Dong, W. Li, W. Guo, H. Wang, S. Wang, J. Tan, Y. Tu, J. Chang, *ACS Appl. Mater. Interfaces* **2015**, *7*, 18997; d) W. Guo, X. Sun, O. Jacobson, X. Yan, K. Min, A. Srivatsan, G. Niu, D. O. Kiesewetter, J. Chang, X. Chen, *ACS Nano* **2015**, *9*, 488.

[11] X. He, J. Gao, S. S. Gambhir, Z. Cheng, *Trends Mol. Med.* **2010**, *16*, 574.

[12] a) Q. Xu, L. M. Ensign, N. J. Boylan, A. Schön, X. Gong, J.-C. Yang, N. W. Lamb, S. Cai, T. Yu, E. Freire, *ACS Nano* **2015**, *9*, 9217; b) C. D. Walkey, J. B. Olsen, H. Guo, A. Emili, W. C. Chan, *J. Am. Chem. Soc.* **2012**, *134*, 2139; c) R. Duncan, *Nat. Rev. Cancer* **2006**, *6*, 688; d) Y. Li, R. Lin, L. Wang, J. Huang, H. Wu, G. Cheng, Z. Zhou, T. MacDonald, L. Yang, H. Mao, *J. Mater. Chem. B* **2015**, *3*, 3591.

[13] a) M. Calderón, M. A. Quadir, S. K. Sharma, R. Haag, *Adv. Mater.* **2010**, *22*, 190; b) Q. Wei, T. Becherer, S. Angioletti-Uberti, J. Dzubiella, C. Wischke, A. T. Neffe, A. Lendlein, M. Ballauff, R. Haag, *Angew. Chem. Int. Ed.* **2014**, *53*, 8004; c) Y. Deng, J. K. Saucier-Sawyer, C. J. Hoimes, J. Zhang, Y.-E. Seo, J. W. Andrejecsk, W. M. Saltzman, *Biomaterials* **2014**, *35*, 6595; d) S. Reimann, D. Gröger, C. Kühne, S. B. Riese, J. Dernedde, R. Haag, *Adv. Healthcare Mater.* **2015**, *4*, 2154; e) Q. Qu, X. Ma, Y. Zhao, *Nanoscale* **2015**, *7*, 16677.

[14] a) A. P. Schenning, C. Elissen-Roman, J.-W. Weener, M. W. Baars, S. J. van der Gaast, E. Meijer, *J. Am. Chem. Soc.* **1998**, *120*, 8199; b) W.-I. Hung, C.-H. Chang, Y.-H. Chang, P.-S. Wu, C.-B. Hung, K.-C. Chang, M.-C. Lai, S.-C. Hsu, Y. Wei, X.-R. Jia, *Langmuir* **2013**, *29*, 12075; c) B. N. Thota, L. H. Urner, R. Haag, *Chem. Rev.* **2015**, *116*, 2079.

[15] a) S. Marrache, S. Dhar, *Proc. Natl. Acad. Sci. USA* **2012**, *109*, 16288; b) C. W. T. Leung, Y. Hong, S. Chen, E. Zhao, J. W. Y. Lam, B. Z. Tang, *J. Am. Chem. Soc.* **2012**, *135*, 62; c) S. Marrache, S. Dhar, *Chem. Sci.* **2015**, *6*, 1832; d) H. S. Jung, J. Han, J.-H. Lee, J. H. Lee, J.-M. Choi, H.-S. Kweon, J. H. Han, J.-H. Kim, K. M. Byun, J. H. Jung, *J. Am. Chem. Soc.* **2015**, *137*, 3017.

[16] X. Wang, N. Shao, Q. Zhang, Y. Cheng, *J. Mater. Chem. B* **2014**, *2*, 2546.

[17] S. Roller, H. Zhou, R. Haag, *Mol. Diversity* **2005**, *9*, 305.

[18] a) S. Biswas, N. S. Dodwadkar, A. Piroyan, V. P. Torchilin, *Biomaterials* **2012**, *33*, 4773; b) R. Mo, Q. Sun, J. Xue, N. Li, W. Li, C. Zhang, Q. Ping, *Adv. Mater.* **2012**, *24*, 3659; c) M. Kodiha, Y. M. Wang, E. Hutter, D. Maysinger, U. Stochaj, *Theranostics* **2015**, *5*, 357.

[19] F. Paulus, M. E. Weiss, D. Steinhilber, A. N. Nikitin, C. Schütte, R. Haag, *Macromolecules* **2013**, *46*, 8458.

[20] D. Gröger, F. Paulus, K. Licha, P. Welker, M. Weinhart, C. Holzhausen, L. Mundhenk, A. D. Gruber, U. Abram, R. Haag, *Bioconjugate Chem.* **2013**, *24*, 1507.